Pramāṇa, Vol. 8, No. 4, 1977, pp. 348–362. © Printed in India.

# Cuspidal edges for elastic wave surfaces for cubic crystals

JACOB PHILIP and K S VISWANATHAN
Department of Physics, University of Kerala, Kariavattom, Trivandrum 695581

MS received 12 November 1976; in revised form 15 January 1977

**Abstract.** The paper deals with a detailed numerical study of the sections of the inverse and ray velocity surfaces for cubic crystals. The figures for the sections of the inverse and ray surfaces by the (001) and (110) planes have been plotted for over 65 crystals and from these, the nature of the cuspidal edges has been discussed. Typical graphs of the inverse and ray surfaces have been given. The parameters characterising the dimensions of the cusps have been tabulated. It is shown that the A–15 compounds exhibit very unusual and interesting wave surfaces at temperatures below superconducting critical temperatures.

**Keywords.** Cuspidal edges; inverse surface; ray surface; A–15 Compounds.

## 1. Introduction

Elastic wave propagation is highly anisotropic in crystals and waves propagate with different velocities in different directions. Except for certain special directions, waves are not strictly transverse or longitudinal in crystals. The group velocity of the waves, with which energy is transported, is generally different both in direction as well as in magnitude from the phase velocity.

The elastic wave surfaces have recently been studied (Brugger 1965, Musgrave 1970, Waterman 1959, Farnell 1961) and the ray surface exhibits cuspidal edges for a large number of crystals. When a cuspidal edge occurs for the ray surface, there exists two or three wave vectors corresponding to a single group velocity vector. Not all crystals give rise to a cusp and the conditions for the existence of cuspidal edges have been derived by Musgrave (1957, 1970), Mc Curdy (1974) and others. Mc Curdy (1974) has pointed out that the directions along which cuspidal edges occur might give rise to high phonon amplification.

The sections of the ray surface as well as the inverse velocity surface by the principal planes of the crystals have been plotted by Miller *et al* (1956), Auld (1973) and others. Generally, these studies were confined to isolated examples of substances which interested the authors, and no systematic study on the different possible patterns of the elastic wave surfaces as well as their unusual or peculiar features have been attempted before. In this paper, we have made an elaborate numerical study of the nature of the inverse and ray surfaces for the (001) and (110) planes for over 65 cubic crystals. Very little work on the nature of the

sections of the ray surface by the (110) plane and the cuspidal edges for this plane has been done earlier. The object of the present paper is to tabulate the substances which exhibit cuspidal edges, the directions along which cusps occur, and to give details of the parameters which characterize the dimensions of the cusp. Such a study will help to classify substances which have striking or anomalous elastic properties and distinguish them from crystals which behave almost as isotropic substances.

It is shown that the A-15 compounds display very interesting elastic properties at low temperatures. They show very large cuspidal edges, and for $Nb_3Sn$, the sections of the inverse and ray surfaces by both planes are unique and are different from the wave surfaces for any other substance reported earlier.

## 2. Wave propagation along the (001) plane

Let $\boldsymbol{k}\,(k_x, k_y, k_z)$ and $\omega$ denote the wave vector and the frequency of the wave respectively. The wave velocity $\mathbf{V}$ is given by $\mathbf{V} = \omega/k$. We denote the direction $(\hat{k}/k)$ of the wave vector by $\hat{n}$ and its components by $(l, m, n)$. The equation for elastic wave propagation for cubic crystals is given by:

$$\begin{vmatrix} C_{11}k_x^2+C_{44}(k_y^2+k_z^2)-\rho\omega^2 & (C_{12}+C_{44})k_xk_y & (C_{12}+C_{44})k_xk_z \\ (C_{12}+C_{44})k_xk_y & C_{11}k_y^2+C_{44}(k_x^2+k_z^2)-\rho\omega^2 & (C_{12}+C_{44})k_yk_z \\ (C_{12}+C_{44})k_xk_z & (C_{12}+C_{44})k_yk_z & C_{11}k_z^2+C_{44}(k_x^2+k_y^2)-\rho\omega^2 \end{vmatrix} = 0 \tag{1}$$

In this section we will specifically consider wave propagation in the $XY$ or the (001) plane. It is well known that for propagation in the $XY$ plane, one mode is a pure shear mode and the other two modes are quasi-shear and quasi-longitudinal. The wave velocities of the three types of elastic wave fronts are given by (Auld 1973)

$$(1/V)_1 = (\rho/C_{44})^{\frac{1}{2}} \tag{2 a}$$

for pure shear wave polarized along the $Z$-axis,

$$(1/V)_2 = (2\rho)^{\frac{1}{2}}\{C_{11} + C_{44} - [(C_{11} - C_{44})^2 \cos^2 2\phi + (C_{12} + C_{44})^2 \sin^2 2\phi]^{\frac{1}{2}}\}^{-\frac{1}{2}} \tag{2 b}$$

for quasi-shear wave, and

$$(1/V)_3 = (2\rho)^{\frac{1}{2}}\{C_{11} + C_{44} + [(C_{11} - C_{44})^2 \cos^2 2\phi + (C_{12} + C_{44})^2 \sin^2 2\phi]^{\frac{1}{2}}\}^{-\frac{1}{2}} \tag{2 c}$$

for quasi-longitudinal wave. In the above equations, $\phi$ is the angle which the wave vector makes with the $X$-axis.

If we write the dispersion eq. (1) in the form

$$\Omega\,(\omega, k_x, k_y, k_z) = 0 \tag{3}$$

the group velocity of the elastic waves is given by (Auld 1973)

$$V_g = -\nabla_k\,\Omega/(\partial\Omega/\partial\omega). \tag{4}$$

The group velocity denotes also the velocity with which the energy of the wave field is transported and the components of the group velocity for wave propagation in the $XY$ plane are given by

$$-\frac{\partial\Omega}{\partial k_y} = -2C_{11}k_x(C_{11}k_y^2 + C_{44}k_x^2 - \rho\omega^2) - 2C_{44}k_x(C_{11}k_x^2 + C_{44}k_y^2 - \rho\omega^2) + 2(C_{12}+C_{44})^2 k_x k_y^2 \quad (5a)$$

$$-\frac{\partial\Omega}{\partial k_y} = -2C_{11}k_y(C_{11}k_x^2 + C_{44}k_y^2 - \rho\omega^2) - 2C_{44}k_y(C_{11}k_y^2 + C_{44}k_x^2 - \rho\omega^2) + 2(C_{12}+C_{44})^2 k_y k_x^2 \quad (5b)$$

$$-\frac{\partial\Omega}{\partial k_z} = 0 \quad (5c)$$

$$\frac{\partial\Omega}{\partial\omega} = -2\rho\omega\{(C_{11}+C_{44})k^2 - \rho\omega^2\}. \quad (5d)$$

If we introduce the vector $\boldsymbol{m}$ such that

$$\boldsymbol{m} = \hat{\boldsymbol{n}}/V \quad (6)$$

having the direction of the wave normal and magnitude equal to the reciprocal of the phase velocity, $\boldsymbol{m}$ is known as the reciprocal velocity vector or slowness vector. The $(1/V)$ surface is called the reciprocal velocity surface and it denotes the locus of the end points of the radius vectors whose lengths are proportional to the refractive indices. Corresponding to the three types of elastic wave fronts propagating along any direction, one can draw three reciprocal wave velocity surfaces, which we shall denote by $L$, $T_1$ and $T_2$ corresponding to the quasi-longitudinal, pure shear and quasi-shear modes given by (2 *c*), (2 *a*) and (2 *b*) respectively.

On the contrary, the ray surface is the locus of points reached at time $t = 1$ by a wave disturbance arising from the origin at $t = 0$, and this surface consists of points reached by the energy of the wave disturbance at a given instant. As stated earlier, the ray velocity or the velocity of transport of energy is identical with the group velocity of the waves and the components of the ray velocity are determined by eqs (4) and (5). Using an IBM 1620 computer the components of the inverse wave velocities of elastic waves propagating in the $XY$ plane for over 65 crystals belonging to the cubic class have been calculated and their inverse wave and ray surfaces plotted. The computations were undertaken with a view to understand the general nature of the elastic wave surfaces and to bring out the geometrically interesting features in these curves. The calculations were made in intervals of 5° for the angle which the wave vector makes with the $X$-axis. Unless otherwise stated, the elastic constant and density data were taken from the reviews of Federov (1968), Auld (1973), Testardi (1973) and Hearmon (1966, 1969). For the ray surfaces, a large number of these crystals were found to exhibit cuspidal edges either along the $X$-axis or along the diagonal line. In fact, the graphs for the energy surfaces were found to fall into three typical patterns as follows:

(i) Some crystals exhibit cuspidal edges along the $X$ and $Y$ axis. Examples of crystals with such cuspidal edges are: Cu, Ag, Au, Fe, Pb, Li, Na, K, Ir, Ge, Si, GaAs, InAs, InP, GaSb, InSb, GaP, ZnS, LiF, Pb $(NO_3)_2$, $MgAl_2O_4$, β-brass, MgO, non-transforming $V_3Si$ at 4·2 K, non-transforming $Nb_3Sn$ at 4·2 K

and $V_3Ge$ at 4·2 K. This list contains a large number of metals and semiconductors.

(ii) Some substances have cuspidal edges along the diagonal or the (110) direction. Examples for such substances are: $NH_4Cl$, CsI, KI, NaCl, AgBr, TlBr, KCN, $NaClO_3$, $UO_2$, RbF, $Bi_{12}GeO_{20}$, transforming $Nb_3Sn$ at 4·2 K, non-transforming $Nb_3Sn$ at 300 K, etc. A large number of ionic crystals were found to exhibit cuspidal edges along the diagonal direction.

(iii) The elastic wave propagation is nearly isotropic in the $XY$ plane, without any cuspidal edges for a large number of crystals and examples for such crystals are: Al, Mo, W, V, Nb, $BaF_2$, $NaBrO_3$, $Sr(NO_3)_2$, $Fe_3O_4$, $Bi_4Ge_3O_{12}$, $FeCr_2O_4$, CaO, $Y_3Al_5O_{12}$ (YAG), $C_6H_{12}N_6$, $SrTiO_3$, $KAlSO_4$, $CH_3$–$NH_3$–$GaSO_4$, $C_4H_4N_2$ $V_3Ge$ at 300 K, PbS, diamond, transforming and non-transforming $V_3Si$ at 300 K and transforming $Nb_3Sn$ at 300 K.

Obviously it is not possible to give the graphs of all the 65 crystals studied due to lack of space. We reproduce in figures 1, 2 and 3 three typical graphs for the substances lithium, rubidium fluoride and tungsten to illustrate the three different types of curves mentioned above. Li has a large cuspidal edge along the $X$-axis. In figure 1, we denote the ratio $AB/OA$ by $\gamma$. Then the semi angle $\theta = \angle PAB$ of the cusp together with the parameter $\gamma$ gives an idea of the dimensions of the cusp and helps one to picture the shape of the energy surface, and the shape of the cusp. The dimensions of the cusp differ from crystal to crystal and the parameter $\gamma$ shows wide variations, starting from near zero values (such as 0·055 for Si), to large values like 5·00 for $V_3Si$, and it assumes the value infinity for non-transforming $Nb_3Sn$ at 4·2 K (table 1).

Figure 2 illustrates the ray and inverse surfaces of RbF which has a cusp along the diagonal or (110) direction. For RbF the ratio $AB/OA = \gamma$ is equal to 0·211 and the semi angle of the cusp is 63°. From table 1 we note that the $\gamma$ values rarely exceed unity in this case. Figure 3 gives the ray and inverse surfaces of W which is nearly isotropic having no cuspidal edges either along the (100) or (110) direction. The $T_1$ and $T_2$ velocity curves are identical over the entire plane and the corresponding ray surfaces almost coincide. A good number of crystals studied show a section of the ray surface having this shape.

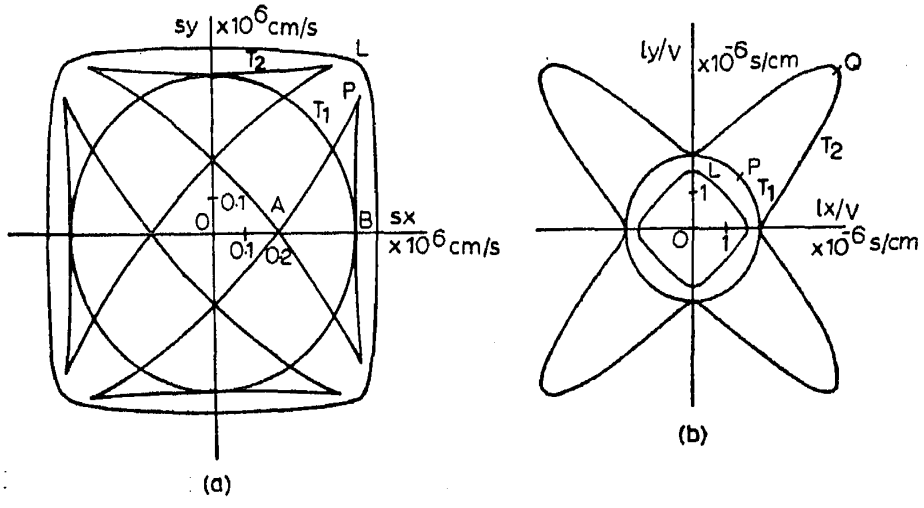


**Figure 1.** (*a*) Section of the ray velocity surface for lithium in the (C01) plane (*b*) Section of the inverse velocity surface for lithium in the (001) plane.

Table 1. Parameters characterizing the cuspidal edges of cubic crystals.

| Crystal | Wave Propagation along (001) Plane | | | | Wave Propagation along (110) Plane | | | | |
|---|---|---|---|---|---|---|---|---|---|
| | Direction of cusp for the $T_2$ branch | $\gamma$ | $\theta°$ | $\delta$ | Direction of the cusp for the $T_2$ branch | $\gamma_1$ | $\theta_1°$ | $\gamma_2$ | $\theta_2°$ |
| Copper[a] | (100) | 0·270 | 60 | 0·765 | (110) & (001) | 0·129 | 58 | 0·20 | 62 |
| Silver[a] | (100) | 0·251 | 60 | 0·722 | (110) & (001) | 0·145 | 60 | 0·158 | 60 |
| Iron[a] | (100) | 0·272 | 60 | 0·609 | (110) & (001) | 0·075 | 58 | 0·120 | 62 |
| Lead[a] | (100) | 0·480 | 59 | 1·000 | (110) & (001) | 0·180 | 60 | 0·180 | 63 |
| Lithium[a] | (100) | 1·300 | 53 | 2·156 | (110) & (001) | 0·286 | 57 | 0·484 | 60 |
| Sodium[a] | (100) | 1·281 | 50 | 2·227 | (110) & (001) | 0·316 | 57 | 0·455 | 63 |
| Germanium[c] | (100) | 0·094 | 64 | 0·283 | (110) & (001) | 0·029 | 62 | 0·039 | 68 |
| Silicon[c] | (100) | 0·055 | 62 | 0·170 | (110) & (001) | 0·019 | 62 | 0·017 | 65 |
| GaAs[c] | (100) | 0·094 | 64 | 02·61 | (110) & (001) | 0·043 | 59 | 0·053 | 65 |
| InP[c] | (100) | 0·125 | 64 | 0·434 | (110) & (001) | 0·057 | 64 | 0·081 | 63 |
| InSb[c] | (100) | 0·180 | 63 | 0·433 | (110) & (001) | 0·045 | 62 | 0·070 | 64 |
| Zinc-blend[a] | (100) | 0·191 | 60 | 0·536 | (110) & (001) | 0·083 | 62 | 0·103 | 61 |
| $\beta$-brass[b] | (100) | 1·260 | 52 | 2·031 | (110) & (001) | 0·338 | 64 | 0·453 | 61 |
| Spinel[b] | (100) | 0·226 | 62 | 0·655 | (110) & (001) | 0·102 | 57 | 0·116 | 62 |
| $Pb(NO_3)_2$[b] | (100) | 0·264 | 57 | 0·663 | (110) & (001) | 0·113 | 58 | 0·167 | 59 |
| Tra $V_3Si$ 4·2 K[d] | (100) | 5·000 | 46 | 6·641 | (110) & (001) | 0·460 | 54 | 0·565 | 59 |
| Non tra. $V_3Si$ 4·2 K[d] | (100) | 1·250 | 49 | 2·071 | (110) & (001) | 0·333 | 58 | 0·480 | 57 |
| Non tra. $Nb_3Sn$ 4·2 K[d] | (100) | .. | 45 | 0·000 | (110) & (001) | 0·478 | 52 | 0·605 | 53 |
| Aluminium[a] | No cusp | .. | .. | .. | No cusp | .. | .. | .. | .. |

| | | | | | | | | | |
|---|---|---|---|---|---|---|---|---|---|
| Vanadium[a] | No cusp | .. | .. | .. | No cusp | .. | .. | .. | .. |
| Ba $F_2$[a] | No cusp | .. | .. | .. | No cusp | .. | .. | .. | .. |
| Pb S[a] | No cusp | .. | .. | .. | No cusp | .. | .. | .. | .. |
| Tungsten[a] | No cusp | .. | .. | .. | No cusp | .. | .. | .. | .. |
| Bismuth Germanate[b] | No cusp | .. | .. | .. | No cusp | .. | .. | .. | .. |
| Chromite[b] | No cusp | .. | .. | .. | No cusp | .. | .. | .. | .. |
| $SrTi O_3$[c] | No cusp | .. | .. | .. | No cusp | .. | .. | .. | .. |
| Diamond[a] | No cusp | .. | .. | .. | No cusp | .. | .. | .. | .. |
| Tra $V_3$ Si 300 K[d] | No cusp | .. | .. | .. | No cusp | .. | .. | .. | .. |
| Non tra $V_3$ Si 300 K[d] | No cusp | .. | .. | .. | No cusp | .. | .. | .. | .. |
| Tra $Nb_3Sn$ 300 K[d] | No cusp | .. | .. | .. | No cusp | .. | .. | .. | .. |
| $V_3Ge$ 300 K[d] | No cusp | .. | .. | .. | No cusp | .. | .. | .. | .. |
| $NH_4Cl$[a] | (110) | 0·096 | 64 | 0·250 | (111) only | 0·049 | 71 | .. | .. |
| KI[a] | (110) | 0·381 | 61 | 0·769 | (111) onlp | 0·250 | 61 | .. | .. |
| KCN[a] | (110) | 0·261 | 60 | 0·587 | (111) only | 0·208 | 58 | .. | .. |
| NaCl[b] | (110) | 0·116 | 60 | 0·378 | (111) only | 0·052 | 63 | .. | .. |
| RbF[a] | (110) | 0·211 | 63 | 0·264 | (111) only | 0·133 | 62 | .. | .. |
| Bismuth Germanium Oxide[b] | (100) | 0·154 | 62 | 0·406 | (111) only | 0·064 | 67 | .. | .. |
| Uranium Oxide[b] | (110) | 0·163 | 64 | 0·464 | (111) only | 0·102 | 65 | .. | .. |
| Tra $Nb_3$ Sn 4·2 K[d] | (110) | 0·591 | 60 | 1·206 | (111) only | 0·482 | 59 | .. | .. |
| Non tra NbS 300 K[d] | (110) | 0·171 | 61 | 0·340 | (111) oniy | 0.039 | 70 | .. | .. |
| $V_3Ge$ 4·2 K[d] | (110) | 0·041 | 63 | 0·194 | (111) only | 0·043 | 71 | .. | .. |

[a] Elastic Constant data from Federov (1968).
[b] Elastic Constant data from Hearmon (1966) and (1969).
[c] Elastic Constant data from Auld (1973).
[d] Elastic Constant data from Testardi (1973).

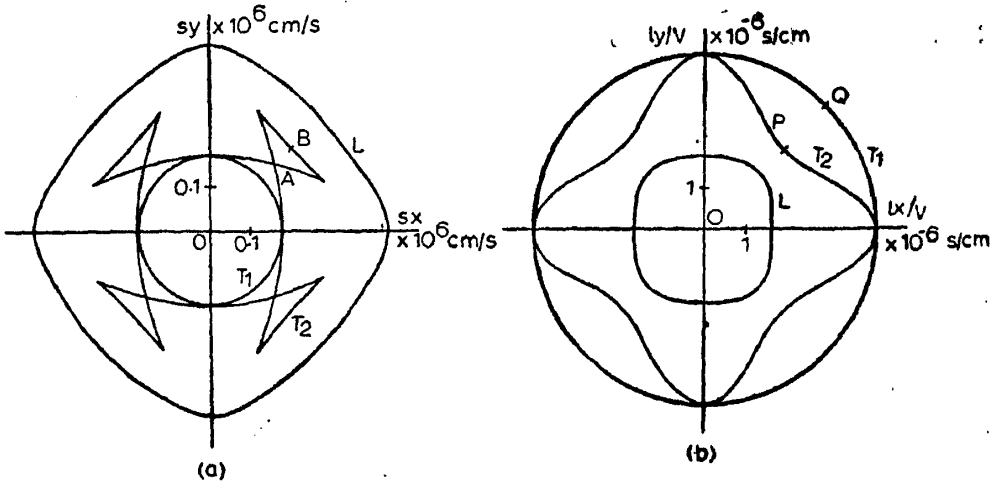


**Figure 2.** (*a*) Section of the ray velocity surface for RbF in the (001) plane. (*b*) Section of the inverse velocity surface for RbF in the (001) plane.

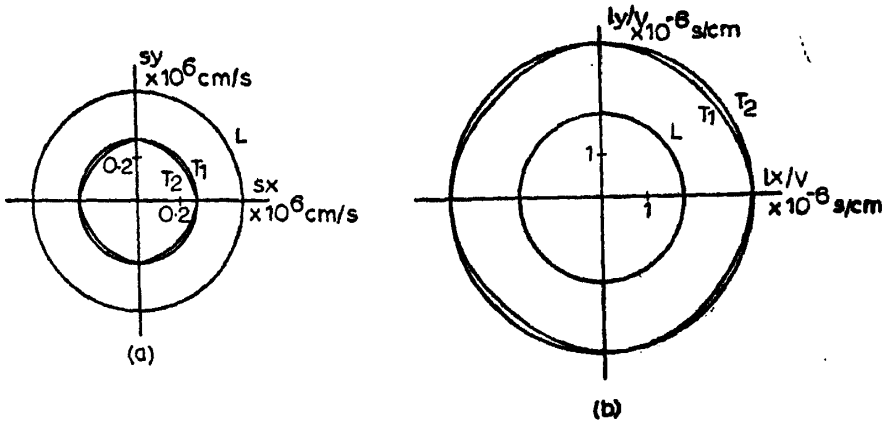


**Figure 3.** (*a*) Section of the ray velocity surface for tungsten in the (001) plane. (*b*) Section of the inverse velocity surface for tungsten in the (001) plane.

In figure 1 it may be noted that $L$ is the innermost of the three inverse wave surfaces showing that quasi-longitudinal wave velocity is generally the highest among the velocities of the three elastic wave fronts. Further, $T_2$ surface contains the $T_1$ surface. It has been found by an inspection of the graphs that if a substance shows a cuspidal edge along the $X$-axis, then the $T_2$ (quasi-shear) slowness surface has a characteristic shape and is stretched out along the diagonal. There is a direct relationship between the magnitude of the maximum along the diagonal in the inverse surface to the dimensions of the cusp. The latter is larger if the stretching is higher, and *vice versa*. To show this we have calculated the parameter $\delta = PQ/OP$ which denotes the stretching of the $T_2$ curve along the diagonal for 23 crystals which exhibit cuspidal edges along the (100) direction and plotted $\gamma$ *versus* $\delta$ in a graph. It has been found that the points almost fall along a curve, which is parabolic near the origin and linear for larger values of $\gamma$. The curve is shown in figure 4 (thick line).

Besides, we calculated the correlation coefficient given by

$$\rho_{corr} = \Sigma\gamma_i\,\delta_i/(\Sigma\gamma_i^2)^{\frac{1}{2}}\,(\Sigma\delta_i^2)^{\frac{1}{2}} \qquad (7)$$

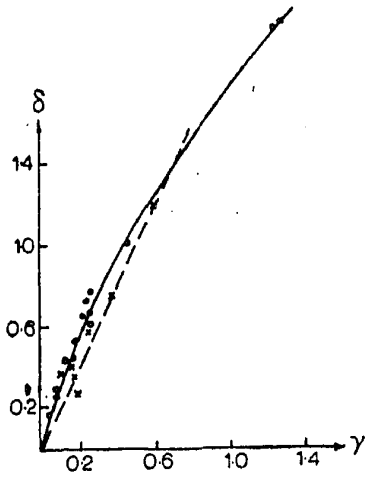


**Figure 4.** Variation of $\delta$ with $\gamma$ (thick line for substances having cusp along the $X$-axis and dotted line for substances having cusp along the diagonal direction).

for these two parameters $\gamma$ and $\delta$ and it was found that $\rho_{corr.} = 0{\cdot}987$. This proves that the degree of stretching in the inverse surface along the diagonal direction is highly correlated to the dimensions of the cusp for the ray surface. The stretching depends on the anisotropy factor $A = 2C_{44}/(C_{11} - C_{12})$. For substances for which $A$ exceeds unity, the curves for the inverse velocity surface are stretched further along the diagonal direction, while for substances for which $A < 1$, they are contracted inwards along the same direction.

In figure 2 for RbF, $T_2$ is contained in $T_1$. In figure 2 we see that curves for the inverse surface for which $T_2$ (quasi-shear) is contained in $T_1$ (pure shear) and further has a minimum along the diagonal, exhibit a cusp in the ray surface along the (110) direction. The parameter $\delta = OP/OQ$ which is a measure of the contraction of the $T_2$ inverse surface has been measured for crystals with cusp along the (110) direction, and the $\gamma$ *vs* $\delta$ graph is plotted which is a straight line as shown in figure 4 (dotted line). The correlation coefficient was calculated and is found to be $0{\cdot}982$ which shows that $\gamma$ is highly correlated to $\delta$ in this case also.

It is well known that the vibration directions of the quasi longitudinal and quasi transverse elastic waves are obliquely inclined to their directions of propagation. For propagation in the $XY$ plane, the vibration direction of the quasi longitudinal mode makes a small angle with the direction of propagation. In order to ascertain whether the departure from longitudinality of the waves is correlated with the presence of large cusps, we selected 25 crystals from the list given in table 1, and our list contained representatives of all the three types mentioned above, *viz.*, crystal in which ray surfaces are isotropic, and crystals that have cuspidal edges along the $X$-axis or along the diagonal direction. The angle which the vibration direction makes with the direction of propagation was calculated throughout the $XY$ plane for all these crystals. These were obtained making use of the following expressions (Miller *et al* 1956) for the amplitudes of vibration for plane waves along the $X$ and $Y$ directions.

$$A_x = \frac{\rho V^2 - C_{44} - (C_{11} - C_{44})\, m^2}{\{(C_{12} + C_{44})^2\, l^2 m^2 + [\rho V^2 - C_{44} - (C_{11} - C_{44})\, m^2]^2\}^{\frac{1}{2}}} \qquad (8\,a)$$

$$A_y = \frac{lm\,(C_{12} + C_{44})}{\{(C_{12} + C_{44})^2\, l^2 m^2 + [\rho V^2 - C_{44} - (C_{11} - C_{44})\, m^2]^2\}^{\frac{1}{2}}}. \qquad (8\,b)$$

Then the angle which the vibration direction makes with the direction of propagation is given by

$$\cos\beta = lA_x + mA_y. \tag{9}$$

It was found that the maximum angle $\beta_{max}$ which the vibration direction makes with the wave vector varied from 1° to 18°. We give in figure 5 the variation of $\beta$ with the direction of propagation $\phi$ for the quasi-longitudinal branch for Al, KI and GaAs. Also we calculated the correlation coefficient for the variables $\beta_{max}$ and $\gamma$ for about ten crystals having a cusp along the $X$-axis and having values from 0·055 to 5·00. This was found to be $\rho_{(\beta_{max},\gamma)} = 0{\cdot}566$ showing that there is good correlation between the existence of cusps and the departures from longitudinality of the elastic waves.

### 3. The wave surfaces of A-15 compounds

Substances like $V_3Si$, $Nb_3Sn$, $V_3Ge$, etc. with A–15 structure have aroused a lot of interest in recent years, because they exhibit high superconducting critical temperatures and other anomalous properties such as phase transition, elastic softening, etc., at low temperatures (Testardi 1973). Sound wave measurements for these crystals have shown that the elastic mode propagating along the (110) direction with $(1\bar{1}0)$ polarization becomes soft at very low temperatures. Our studies have shown that the elastic wave surfaces for A–15 compounds are very interesting and are unique. From the table we see that $V_3Si$ at 4·2°K has a very high value for $\gamma$ *viz.*, 5·00, which is next only to $Nb_3Sn$ at a temperature of 4·2° K. It has a very large cusp, and the $T_2$ branch of the inverse surface shows a long spike at 45°.

For $Nb_3Sn$ of the non-transforming type, the relation $C_{11} = C_{12}$ holds good at 4·2°K and the spike in the inverse surface extends up to infinity. This is because the $T_2$ mode strictly becomes soft at 4·2°K. As can be seen from figure 6, the energy surface is made up of only cusps and the large cuspidal edges reduce to four straight lines intersecting at the origin. The value of the parameter $\gamma$ tends to infinity. At 300°K, the anisotropy factor A = 0·56 and is less than unity. Hence at this temperature the substance exhibits a cusp along the diagonal direction. However when the temperature is lowered to 4·2° K, the anisotropy factor tends to infinity and this explains why the cusp is directed along the $X$-axis. In fact, the change in the nature of the cusp should occur at a higher critical temperature where A is equal to unity. The A–15 compounds are unique

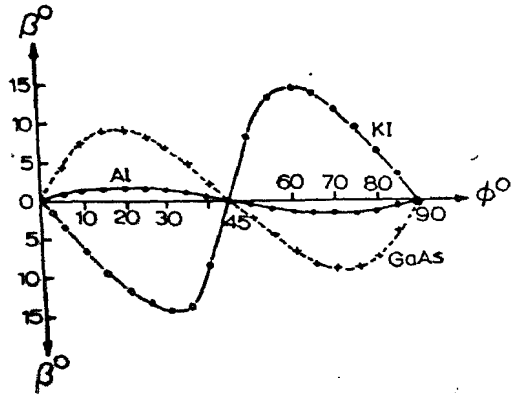


**Figure 5.** Variation of $\beta$ with direction of propagation $\phi$ for Al, KI and GaAs.

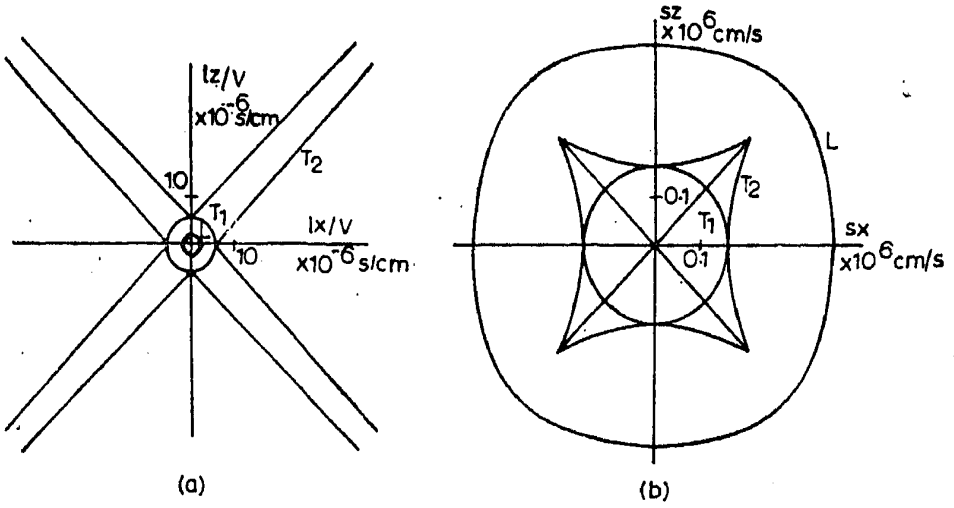


**Figure 6.** (*a*) Inverse velocity surface of $Nb_3Sn$ (non tra.) at 4·2°K in the (001) plane. (*b*) Ray velocity surface of $Nb_3Sn$ (non tra.) at 4·2°K in the (001) plane.

for the very large cuspidal edges that they exhibit at low temperatures. We have plotted the graphs for these substances both at 300°K as well as at 4·2°K and it was found that the wave surfaces show remarkable temperature variations.

It can be shown that if the wave velocity becomes zero, the energy surface should pass through the origin. If $S_x$ and $S_y$ denote the components of the energy velocity along the $X$ and $Y$ axis, it follows from eqs (4) and (5) that

$$\frac{S_x}{l} + \frac{S_y}{m} = -\frac{\rho V (C_{11} + C_{44})}{(C_{11} + C_{44}) - \rho V^2} \cdot \tag{10}$$

For shear mode propagating along the (110) direction, the wave velocity is given by

$$\rho (\omega/k)^2 = \rho V^2 = (C_{11} - C_{12})/2 \tag{11}$$

and becomes zero at 4·2°K for $Nb_3Sn$. So the right hand side vanishes and the section of the energy surface in the $XY$ plane degenerates into the straight lines

$$S_x \pm S_y = 0 \tag{12}$$

in the neighbourhood of the origin. The energy surface for the $T_2$ branch should thus pass through the origin and reduce to straight lines inclined at 45° with the axes. The numerical calculations, as depicted in figure 6 confirm this finding.

## 4. Wave propagation along the (110) plane

Next we consider the nature of the sections of the inverse and ray surfaces by the (110) plane which contains the face and cube diagonals of the unit cube. Numerical work on wave propagation has generally been confined to the principal cubic planes of the crystal and very few studies have been made on the nature of the ray velocity surfaces along the (110) plane. A unit vector lying in the (110) plane has direction cosines ($l$, $l$, $n$) so that

$$2l^2 + n^2 = 1 \text{ or } k_x^2 = k^2 (1 - 2k_x^2/k^2) \tag{13}$$

By substituting $k_x = k_y = lk$ and $k_z = k(1 - 2k_x^2/k^2)^{\frac{1}{2}}$ in eq. (1), we can obtain the dispersion relation for the propagation of a wave along a general direction in this plane. The dispersion relation (1) can now be written as

$$\Omega = X^3 + A_1X^2 + A_2X + A_3 \tag{14}$$

where

$$X = \rho V^2 = \rho\,(\omega/k)^2.$$

The coefficients $A_1$, $A_2$ and $A_3$ are related to the elements of the matrix given by (1). Let us denote the $(i, j)$th element of this matrix by $\alpha_{ij}$, and let $a_{ij} = (\alpha_{ij}/k^2)$. Let us denote by $A_{ij}$ the cofactors of the elements of the matrix $A = (a_{ij})$ and by $\triangle$, the determinant of this matrix. Then one can find that

$$A_1 = a_{11} + a_{22} + a_{33}$$
$$A_2 = A_{11} + A_{22} + A_{33}$$
$$A_3 = \triangle.$$

By direct differentiation, we find that

$$\frac{1}{k^5}\frac{\partial\Omega}{\partial k_x} = \frac{1}{k^5}\frac{\partial\Omega}{\partial k_y} = -2\,(\rho V^2)^2\,(C_{11} + 2C_{44})\,l +$$
$$2\,(\rho V^2)\,[C_{44}\,(a_{22} + a_{33} + 2a_{11})\,l + C_{11}\,(a_{22} + a_{33})\,l -$$
$$(C_{12} + C_{44})\,(a_{12}\,l + a_{13}\,n)] - 2\,[C_{44}\,(a_{11}\,a_{22} + a_{11}\,a_{33} - a_{13}^2$$
$$- a_{12}^2)\,l + C_{11}\,(a_{22}\,a_{33} - a_{23}^2)\,l + (C_{12} + C_{44})\,(a_{22}\,a_{23}n +$$
$$a_{13}\,a_{23}l - a_{12}a_{33}l - a_{13}a_{22}n)] \tag{15a}$$

$$\frac{1}{k^5}\frac{\partial\Omega}{\partial k_z} = -2\,(\rho V^2)^2\,(C_{11} + 2C_{44})\,n + 2\,(\rho V^2)\,[C_{44}\,(a_{11} + a_{22}$$
$$2a_{33})\,n + C_{11}\,(a_{11} + a_{22})\,n - (C_{12} + C_{44})\,(a_{13} + a_{23})\,l] -$$
$$- 2\,[C_{44}\,(a_{11}a_{33} + a_{22}a_{33} - a_{23}^2 - a_{13}^2)\,n + C_{11}\,(a_{11}a_{22} - a_{12}^2)\,n$$
$$+ (C_{12} + C_{44})\,(a_{12}a_{13} + a_{12}a_{23} - a_{11}a_{23} - a_{13}a_{22})\,l] \tag{15b}$$

$$\frac{1}{k^5}\frac{\partial\Omega}{\partial\omega} = 2\,(\rho V)\,[3\rho^2V^4 - 2\,(\rho V^2)\,(a_{11} + a_{22} + a_{33}) +$$
$$+ a_{11}a_{22} + a_{11}a_{33} + a_{22}a_{33} - a_{13}^2 - a_{23}^2 - a_{12}^2]. \tag{15c}$$

The components of the group velocity vector $V_g$ along the three principal axes can be obtained from the formula (4). It can be seen from (15) that the component $(V_g^x - V_g^y)/\sqrt{2}$ of $V_g$ along a direction $(1/\sqrt{2} - 1/\sqrt{2}, 0)$ normal to the plane is zero and the group velocity vector for the waves propagating along a general direction lies in the plane itself. We shall call the direction $(1/\sqrt{2}, 1/\sqrt{2}, 0)$ of the face diagonal as the $\xi$-axis. Then the principal axes for this plane can be taken as the $\xi$- and $Z$-axes, and further

$$V_g^\xi = (V_g^x + V_g^y)/\sqrt{2} \tag{16}$$

A computer programme was written to solve the cubic eq. (14) as well as to evaluate the components $V_g^\xi$ and $V_g^z$ given by (15 *a*) and (15 *b*). The three roots of the equation give the three different phase velocities (or their inverses) of the three elastic wave fronts. The computer was instructed to print the values of the three inverse wave velocities as well as the components $V_g^\xi$ and $V_g^z$ of the group velocity vector in intervals of 5° for the direction of propagation in this plane. The correctness of the calculations were checked by comparing the values of

the inverse wave velocities and the components of the group velocities along the direction (110) with the values for the same quantities calculated on the basis of eqs (2) and (5), and these were found to agree up to four or five decimal places. From the computer output data, curves for the inverse and ray surfaces could be plotted. We have plotted these graphs for sixty five crystals for wave propagation in the (110) plane.

It is well known that two of the wave velocities ($T_1$ and $T_2$) of waves propagating along the (111) direction are equal and internal conical refraction can occur for this direction. This fact was numerically verified for all the crystals, and the inverse $T_1$ and $T_2$ surfaces intersect each other at an angle of 36° corresponding to the direction of the cube diagonal in this plane. As in the case of the $XY$ plane, cuspidal edges occur for the $T_2$ wave surface only and a large number of crystals were found to exhibit cuspidal edges either along the $\xi$- and $Z$-axes simultaneously or along the direction of the cube diagonal. The slowness surface for the $T_1$ branch is found to be an ellipse, with its major axis either along the $\xi$-axis or along the $Z$-axis, and this fact is strongly correlated with the nature of the cusps also. For example if the section of the wave surface for the $T_1$ branch is an ellipse with its major axis along the $Z$-axis, in this case the $T_2$ ray surface will exhibit two cuspidal edges along the $\xi$ and $Z$ axes respectively. If, on the other hand, the inverse velocity curve for the $T_1$ branch happens to be an ellipse elongated along the $Z$-axis, the ray surface for the $T_1$ branch will be an ellipse with its major axis along the $\xi$-axis, and in this case, the section of the ray surface for the $T_2$ branch will have a cusp along the direction of the cube diagonal. It has also been found that the dimensions of the cusp are correlated with the eccentricity of the ellipse; the greater the eccentricity, the larger will be the cusp. It is difficult to give the curves for the sections of the inverse and ray surfaces for the 65 crystals. These curves were found to fall into three classes as follows:

(i) More than 25 crystals in the list showed two cusps for the $T_2$ branch, one each along the $\xi$- and $Z$-axes respectively. Examples of these types of crystals are: Cu, Ag, Au, Fe, Li, Na, K, Ge, Si, Ir, GaAs, InAs, InP, GaSb, GaP, ZnS, LiF, $\beta$-brass, $Pb(NO_3)_2$, $MgAl_2O_4$, $V_3Si$ (transforming at 4·2° K) $V_3Si$ (non-transforming at 4·2° K), $Nb_3Sn$ (non-transforming at 4·2° K), etc. The cusps are of varying dimensions for the different crystals. The three curves for the slowness surface were found to have a definite pattern in this case. It is found that the $T_2$ surface contains the $T_1$ surface between the $Z$-axis and the direction of the cube diagonal, and the $T_1$ curve contains the $T_2$ curve between the $\xi$-axis and the direction of the cube diagonal where the two curves intersect. We reproduce in figure 7 the curves for copper to illustrate the types of wave surfaces having two cusps.

(ii) A number of substances exhibit one cusp for the $T_2$ branch along the direction of the cube diagonal for the ray surface. As examples, we may cite the crystals $NH_4Cl$, KI, RbF, NaCl, TlBr, $NaClO_3$, KCN, $UO_2$, CsI, $V_3Ge$ (4·2°K), transforming $Nb_3Sn$ at 4·2°K, etc. For these crystals, the ray surface for the $T_2$ branch is an ellipse with its major axis along the $\xi$-direction and correspondingly the slowness surface for the $T_1$ mode turns out to be an ellipse, with its major axis along the $Z$-direction. For these substances, it is found that the inverse wave surface for $T_2$ will be contained within $T_1$ between the $Z$-axis and the direction of the cube diagonal, and in the region between the cube diagonal and the $\xi$-axis, the reverse will happen. The nature of the curves is just the opposite

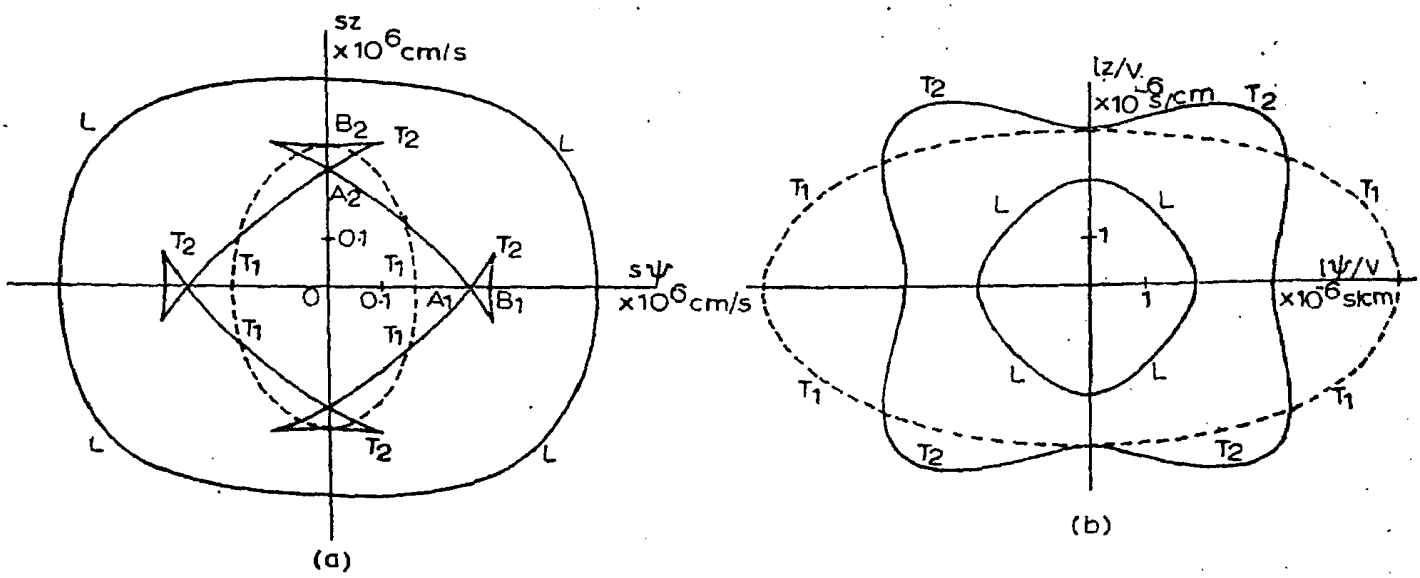


**Figure 7.** (*a*) Section of the ray velocity surface for copper in the (110) plane. (*b*) Section of the inverse velocity surface for copper in the (110) plane.

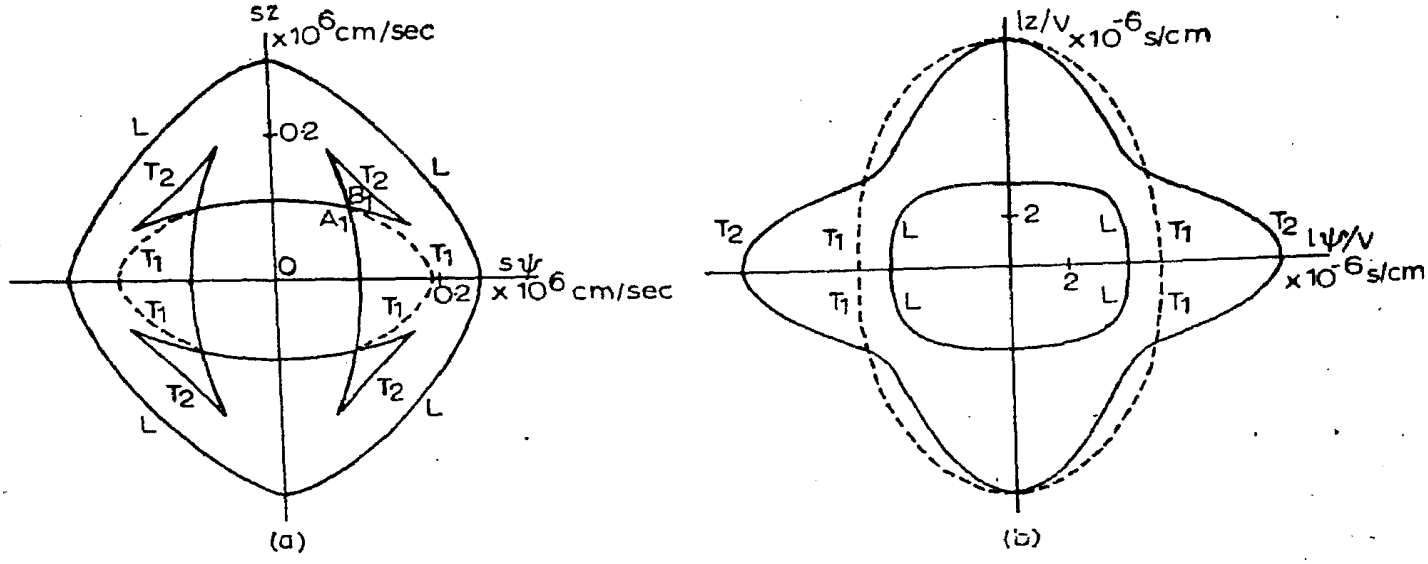


**Figure 8.** (*a*) Section of the ray velocity surface for KI in the (110) plane. (*b*) Section of the inverse velocity surface for KI in the (110) plane.

of the case (i) mentioned above corresponding to two cusps along the $\xi$- and $Z$-axes. We reproduce in figure 8 the ray and inverse surfaces of KI to illustrate this type of wave surfaces.

(iii) A large number of crystals are isotropic, and the curves for both the ray and inverse wave surfaces were nearly circular. Examples are: Al, Mo, W, V, Nb, $BaF_2$, $Sr(NO_3)_2$, $Fe_3O_4$, Bismuth-Germanate, Chromite, Yittrium Aluminium Garnette, $SrTiO_3$, $KAlSO_4$, Succino nitrile, CaO, etc. A typical curve for substances with isotropic wave section is given in figure 9 for the case of BaF.

Lithium, Sodium, Potassium, $\beta$-brass, $V_3Si$ and $Nb_3Sn$ have large cusps along the axes for the $T_2$ branch. In table 1, $\gamma_1 = A_1B_1/OA_1$ (figure 7) and $\gamma_2 = A_2B_2/OA_2$ (figure 7) are the parameters giving the dimensions of the cusps for the $T_2$ branch along (110) and (001) directions respectively; $\theta_1$ and $\theta_2$ are the corresponding semiangles of the cusps. For crystals which exhibit cusp along the (111)

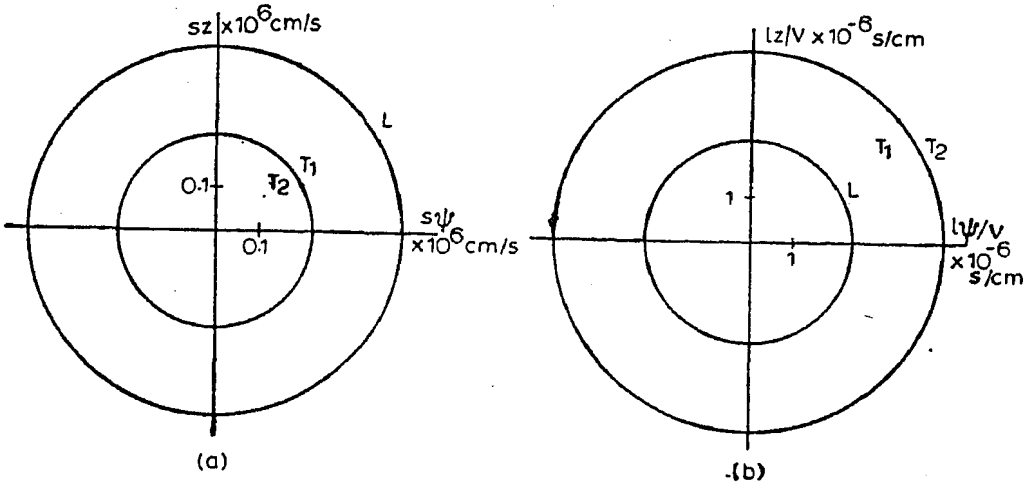


**Figure 9.** (*a*) Section of the ray velocity surface for $BaF_2$ in the (110) plane (*b*) Section of the inverse velocity surface for $BaF_2$ in the (110) plane.

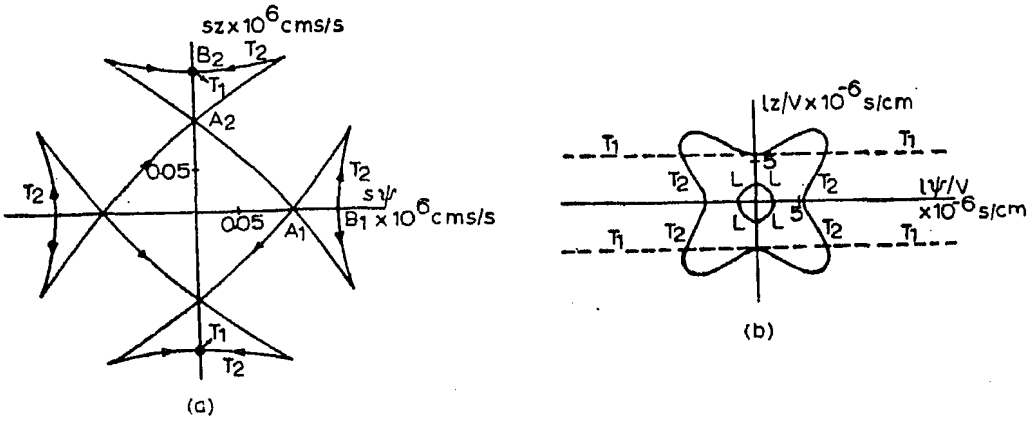


**Figure 10.** (*a*) Section of the ray velocity surface for $Nb_3Sn$ (non tra.) at 4·2°K in the (110) plane ($T_1$ and $T_2$ branches only). (*b*) Section of the inverse velocity surface for $Nb_3Sn$ (non tra.) at 4·2°K in the (110) plane.

direction for the $T_2$-branch, the dimensions and semiangles of the cusps are given as $\gamma_1$ and $\theta_1$ (figure 8) in table 1. For Li, K, Na, $\beta$-brass, $V_3Si$ and $Nb_3Sn$, the values of $\gamma_1$ and $\gamma_2$ are larger, but these never exceed unity, unlike the case of cusps for the (001) plane. The other crystals in the list have relatively smaller cusps.

## 5. Results for A-15 compounds

In the (110) plane also the A–15 compounds distinguish themselves by their unique behaviour and have very interesting wave surfaces. Since the $T_2$ mode becomes soft at low temperatures for propagation along the $\xi$-axis, the computer encountered division by zero along this direction for $Nb_3Sn$ of the non-transforming type but could give values for the other directions. In view of the fact that the components of the phase and group velocities showed steep variation, the computer was made to perform the calculations at intervals of 1° so that the graphs could be correctly drawn. Both the transforming and non-transforming varieties of $V_3Si$ at 4·2°K show two cuspidal edges, one each along the $\xi$ and $Z$ axis. Non-transforming $Nb_3Sn$ at 4·2°K has an almost distinct type of wave surface amongst all the sixty-five crystals considered here. In figure 10 *a*, we give the ray surfaces for $T$

and $T_2$ branches and in figure 10 *b*, the inverse surfaces. It is found that the inverse surface for $T_1$ in this case degenerates into two straight lines, parallel to the $\xi$-axis and symmetrically situated with respect to it, and that the ray surface for the $T_1$ branch reduced just to two points marked with a circle. By the principle of reciprocity, for every tangent line to the inverse surface, there exists a corresponding point lying on the ray surface. Since the tangent line at every point on the $T_1$ branch in this case reduces to the line itself, the ray surface should consist of two points, which are the polar reciprocals of these lines.

The unique nature of the wave surface for the $Nb_3Sn$ can also be proved mathematically. By subtracting the elements of the second row from that of the first in the determinant (1), it can be seen that one of the roots of the equation (1) is given by

$$\rho V^2 = (C_{11} - C_{12})\, l^2 + C_{44} n^2. \tag{17}$$

This explains why the inverse as well as the ray surfaces for the $T_1$ mode are ellipses. Since $C_{11} = C_{12}$, for $Nb_3Sn$ at 4·2° K, it follows from (17) and (6), that the inverse velocity surface reduces to the two lines

$$m_z = \pm (\rho/C_{44})^{\frac{1}{2}} \tag{18}$$

and these are parallel to the $\xi$-axis. Further, one can see from equation (15) that

$$S_x = S_y = S_\xi = 0, \text{ and} \tag{19}$$

$$S_z = \pm (C_{44}/\rho)^{\frac{1}{2}} \tag{20}$$

The component $S_z$ is independent of the direction. The above equation shows that the section of the ray surface by the (110) plane for $Nb_3Sn$ should degenerate to two points situated symmetrically at a distance of $(C_{44}/\rho)^{\frac{1}{2}}$ from the origin along the $Z$-axis.

## Acknowledgement

One of the authors (JP) is grateful to CSIR, New Delhi, for financial assistance in the form of a Junior Fellowship.

## References

Auld B A 1973 *Acoustic Fields and Waves in Solids* Vol. 1 (John Wiley and Sons, New York) Ch. 7

Brugger K 1965 *J. Appl. Phys.* 36 759

Farnell G W 1961 *Can. J. Phys.* 39 65

Federov F I 1968 *Theory of Elastic Waves in Crystals* (Plenum Press, Inc., New York) Chs. 3, 4 and 7

Hearmon R F S 1966 and 1969 in *LANDÖLT—BÖRNSTEIN* (ed. K. H. Hellwege and A. M Hellwege) Vols. 1 and 2 (Springer-Verlag, New York)

Mc Curdy A K 1974 *Phys. Rev.* B9 466

Miller G F and Musgrave M J P 1956 *Proc. R. Soc.* A236 352

Musgrave M J P 1957 *Proc. Cambr. Phil. Soc.* 53 897

Musgrave M J P 1970 *Crystal Acoustics* (Holden-Day, San Francisco) Ch. 6–10

Testardi L R 1973 *Physical Acoustics* Vol. 10 ed. W. P. Mason and R. N. Thurston (Academic Press, New York) p. 193

Waterman P 1959 *Phys. Rev.* 113 1240